Accepted Manuscript

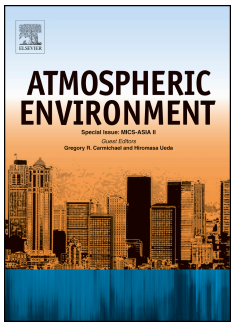

Title: WRF-Chem Simulation of East Asian Air Quality: Sensitivity to Temporal and Vertical Emissions Distributions

Authors: Xueyuan Wang, Xin-Zhong Liang, Weimei Jiang, Zhining Tao, Julian X.L. Wang, Hongnian Liu, Zhiwei Han, Shuyan Liu, Yuyan Zhang, Georg A. Grell, Steven E. Peckham

PII: S1352-2310(09)00955-8

DOI: 10.1016/j.atmosenv.2009.11.011

Reference: AEA 9381

To appear in: *Atmospheric Environment*

Received Date: 6 August 2009

Revised Date: 23October2009

Accepted Date: 6 November 2009

Please cite this article as: Wang, X., Liang, X.-Z., Jiang, W., Tao, Z., Wang, J.X.L, Liu, H., Han, Z., Liu, S., Zhang, Y., Grell, G.A., Peckham, S.E. WRF-Chem Simulation of East Asian Air Quality: Sensitivity to Temporal and Vertical Emissions Distributions, Atmospheric Environment (2009), doi: 10.1016/ j.atmosenv.2009.11.011

This is a PDF file of an unedited manuscript that has been accepted for publication. As a service to our customers we are providing this early version of the manuscript. The manuscript will undergo copyediting, typesetting, and review of the resulting proof before it is published in its final form. Please note that during the production process errors may be discovered which could affect the content, and all legal disclaimers that apply to the journal pertain.

ARTICLE IN PRESS

WRF-Chem Simulation of East Asian Air Quality: Sensitivity to Temporal and Vertical Emissions Distributions

Xueyuan Wang[a,b], Xin-Zhong Liang[b,*], Weimei Jiang[a], Zhining Tao[b,c], Julian X.L. Wang[d], Hongnian Liu[a], Zhiwei Han[e], Shuyan Liu[b], Yuyan Zhang[f], Georg A. Grell[g], Steven E. Peckham[g]

[a]School of Atmosphere Sciences, Nanjing University, Nanjing, China

[b]Division of Illinois State Water Survey, Institute of Natural Resource Sustainability, University of Illinois, Champaign, IL, USA

[c]NASA Goddard Space Flight Center, Greenbelt, MD, USA

[d]NOAA Air Resources Laboratory, Boulder, CO, USA

[e]Institute of Atmospheric Physics, Chinese Academy of Science, Beijing, China

[f]Nanjing Municipal Environment Monitoring Centre Station, Nanjing, China

[g]NOAA Earth System Research Laboratory/Global Systems Division, Boulder, CO, USA

ACCEPTED MANUSCRIPT

[*] Corresponding author: Dr. Xin-Zhong Liang, Postal address: Illinois State Water Survey, University of Illinois at Urbana-Champaign, 2204 Griffith Dr., Champaign, IL 61820-7495. E-mail: xliang@illinois.edu, Voice: 217-244-6864; Fax: 217-244-0220.

Abstract

This study develops fine temporal (seasonal, day-of-week, diurnal) and vertical allocations of anthropogenic emissions for the TRACE-P inventory and evaluates their impacts on the East Asian air quality prediction using WRF-Chem simulations in July 2001 at 30-km grid spacing against available surface measurements from EANET and NEMCC. For NO_2 and SO_2, the diurnal and vertical redistributions of emissions play essential roles, while the day-of-week variation is less important. When all incorporated, WRF-Chem best simulates observations of surface NO_2 and SO_2 concentrations, while using the default emissions produces the worst result. The sensitivity is especially large over major cities and industrial areas, where surface NO_2 and SO_2 concentrations are reduced by respectively 3-7 and 6-12 ppbv when using the scaled emissions. The incorporation of all the three redistributions of emissions simulates surface O_3 concentrations higher by 4-8 ppbv at night and 2-4 ppbv in daytime over broad areas of northern, eastern and central China. To this sensitivity, the diurnal redistribution contributes more than the other two.

Keywords: WRF-Chem; emissions; diurnal cycle; vertical redistribution; air quality modeling; East Asia.

ACCEPTED MANUSCRIPT

1. Introduction

East Asia has experienced continuous rapid economic and population growth during the past three decades. Recent industrialization and urbanization have resulted in substantial increases of anthropogenic emissions, especially from China (Zhang et al., 2007; Ohara et al., 2007). This has caused significant degradation of the air and water quality and thus serious consequences on the environment and ecosystem over the region. East Asian pollutants can also affect the biogeochemical cycle and climate change at regional to global scales (Akimoto, 2003). Through long-range transport, these pollutants have important impacts on the air quality over the North Pacific and North America (Jacob et al., 1999; Wang et al., 2009). As a fundamental tool to quantify these issues, air quality modeling over East Asia has drawn increasing efforts.

For air quality modeling, a basic but crucial factor is the specification of accurate emissions inventories (Placet et al., 2000; Kurata et al., 2004). The current inventories are characterized by two major uncertainties: the total amount of each pollutant emitted, and its temporal and spatial (horizontal and vertical) distribution. Modeling studies for USA (Tao et al., 2004), Europe (de Meij et al., 2006), and Mexico (Ying et al., 2009) have shown the sensitive role of temporal allocation of emissions. Altering emissions distribution, while keeping the total amount unchanged, has significant impacts on air quality prediction. This scaling issue is especially important for East Asia, where the best available emissions data contain mostly estimates of only annual or seasonal totals.

Currently, two major regional emissions inventories are available for East Asia. They are the Regional Emission Inventory in Asia (REAS) version 1.1, constructed by Ohara et al. (2007), and the NASA Transport and Chemical Evolution over the Pacific (TRACE-P) emissions inventory developed by Streets et al. (2003a). The REAS inventory is not sufficient for use in

ACCEPTED MANUSCRIPT

this study because it contains only annual total emissions with no temporal variations for individual source categories. The TRACE-P inventory considers seasonal dependence of emissions for certain source categories and has been widely used in recent modeling studies of East Asian air quality (Carmichael et al., 2008; Han et al., 2008). However, it still lacks resolution of temporal allocations at shorter but critical (e.g., day-of-week, diurnal) scales. Finer-resolution temporal allocations have been derived in some inventories in limited areas, including a part of eastern China (Wang et al., 2005) and Japan (Kannari et al., 2007). None of these inventories provides information on the vertical distribution of emissions that has important impacts on air quality modeling (de Meij et al., 2006).

This study first develops fine-resolution temporal (seasonal, day-of-week, diurnal) and vertical allocations specific to source categories and chemical species for the TRACE-P inventory, and then evaluates their individual and combined effects on the East Asian air quality prediction. For the latter, six sensitivity simulations are conducted for July 2001 using Weather Research and Forecasting/Chemistry model (WRF-Chem, Grell et al., 2005) and compared against observations of NO_2, SO_2, and O_3 concentrations to examine the relative contributions among the fine temporal (day-of-week, diurnal) and vertical distributions of anthropogenic emissions while keeping the monthly totals unchanged.

2. Model simulations and observational data

This study uses WRF-Chem version 2.2, a new generation of fully coupled online air quality model (Grell et al., 2005). The model details and relevant publications can be found at http://ruc.fsl.noaa.gov/wrf/WG11/ and http://www.wrf-model.org. The model predicts simultaneous variations of meteorological states (wind, temperature, humidity, precipitation,

ACCEPTED MANUSCRIPT

clouds, etc.), advective, convective, and diffusive transports, radiation and photolysis rates, biogenic emissions, wet and dry depositions, as well as gas-phase and aerosol chemistry.

The chemistry component of WRF-Chem adopts the Fast-J photolysis scheme integrates instant hydrometeors, aerosols, and clouds to calculate 24 photochemical reactions (Fast et al., 2006). Dry deposition is calculated according to Wesely (1989). The gas-phase chemistry adopts the Regional Atmospheric Chemistry Mechanism (RACM, Stockwell et al., 1997). It includes 21 inorganic and 56 organic species and has 237 reactions.

Figure 1 illustrates the model computation domain. It covers the whole China, Japan, and the Korean Peninsula with 232×172 horizontal grid cells at a 30-km spacing by the Lambert conformal map projection centered at (35.18ºN, 110ºE). The model includes 28 vertical layers, with the top at 50 hPa (~19.8 km), about 6 layers within the planetary boundary layer, and the first layer central at ~38 m.

This study conducts six sensitivity simulations to evaluate the individual and combined impacts of the fine temporal and vertical allocations of anthropogenic emissions on East Asian air quality modeling (Table 1). These simulations are forced by identical monthly variations and geographic distributions of total column emissions that are specific for each emission category and chemical species. Although conserving the totals, the actual hourly vertical distribution of the emissions differs among the simulations due to incorporating the day-of-week (W), diurnal (D), and/or vertical (V) allocations. For convenience, the simulations are hereafter identified as E_{id}, where {id} is any combination of {W, D, V}. For example, E_WDV denotes for the simulation using the emissions that include all the day-of-week, diurnal and vertical allocations, while E_N is the control run based on the default monthly emissions with none of the three allocations. Considering the expensive computational demand (~8,000 CPU hours per model

ACCEPTED MANUSCRIPT

month), the sensitivity study here focuses on July as a representative of prevailing high O_3 episodes in summer.

For all simulations, the meteorological initial and boundary conditions are constructed from the National Centers for Environmental Prediction Final Global Analyses data, available every 6 hours at 1°×1° grid spacing resolution. This use of the observational analysis drives the WRF-Chem to reproduce reasonably accurate meteorological conditions. The chemical boundary conditions are specified as that representative of the northern mid-latitude clean environment (Grell et al., 2005). Each simulation starts 7 days earlier, and the initial period (June 24-30) is considered as a model spin-up, from which the output is not used in the subsequent analysis.

Observational data include measurements from the Acid Deposition Monitoring Network in East Asia (EANET) and the National Environmental Monitoring Centre of China (NEMCC). EANET was started in 1998 in several countries, and the data have been widely used for model evaluation (Carmichael et al., 2008; Han et al., 2008). There are 43 EANET sites (Fig. 1), but only 24 sites provide data in the WRF-Chem domain (EANET, 2001). Note that the data availability varies among sites (Table 2), which limits our ability to compare consistently across all quantities. This study utilizes hourly (Japan only) concentrations of NO_x ($NO+NO_2$), SO_2, and O_3, daily (China) and monthly (other sites) mean concentrations of NO_2 and SO_2 from EANET, and daily max 1-hr O_3 concentrations in Beijing from NEMCC (Wang et al., 2009) for July to examine the impacts of emissions temporal and vertical allocations.

The overall model performance is quantified by five statistical measures: correlation coefficient (R), mean bias (MB), normalized bias (NB), gross error (GE), and normalized error (NE). For any given variable with (n) pairs of observed (O) and modeled (P) values, these statistics are defined as follows:

$$\bar{F} \equiv \tfrac{1}{n}\sum_{i=1}^{n} F_i$$

$$R = \sum_{i=1}^{n}(P_i - \bar{P})(O_i - \bar{O}) \Big/ \sqrt{\sum_{i=1}^{n}(P_i - \bar{P})^2 \sum_{i=1}^{n}(O_i - \bar{O})^2}$$

$$MB = \overline{P - O} \quad , \quad NB = \overline{P/O - 1} \quad , \quad GE = \overline{|P - O|} \quad , \quad NE = \overline{|P/O - 1|}$$

They can be calculated from samples among different sites to depict spatial pattern agreement or among different times at individual sites to identify temporal correspondence. A perfect model score would have $R = 1$, $MB = 0$, $NB = 0$, $GE = 0$, $NE = 0$.

3. Emissions inventory

The emissions inventory used in this study consists of four separate sources types: anthropogenic, biomass burning, biogenic, and volcanic emissions. Other natural sources, such as dimethlysulfide (DMS), lightning NO_x, dust, and sea salt, are not included due to the lack of data.

The biogenic emissions of volatile organic compounds (VOCs) are predicted online by WRF-Chem according to Guenther et al. (1994). The biomass burning emissions are the TRACE-P estimate of typical monthly profiles (Streets et al., 2003b). The volcanic SO_2 emissions erupted from Miyakejima (139.53ºE, 34.08ºN, 813 m MSL) are derived from Kajino et al. (2004). The eruption began from July 2000, decreased over time in 2001, and increased again in March 2002. The volcanic sulfate contributed insignificantly to Japan air quality in July 2001 (Kajino et al., 2004). The biogenic and biomass burning emissions are allocated in the 1st (bottom) model layer, while the volcanic emissions are placed in the 5th model layer (~925 hPa, approximating the estimated smoke height between 450 and 760 m) for all simulations.

The anthropogenic emissions are taken from the TRACE-P inventory (Streets et al., 2003a). This inventory is considered the standard by the Model Intercomparison Study Asia Phase II (MICS-Asia II) project (Carmichael et al., 2008; Han et al., 2008). It includes 10 primary species

ACCEPTED MANUSCRIPT

(SO_2, NO_x, CO, CO_2, CH_4, NH_3, PM_{10}, $PM_{2.5}$, black carbon [BC], and organic carbon [OC]) and 19 subcategories of non-methane volatile organic compounds (NMVOC). Emissions of each species are split into area sources and large point sources (LPSs). Area sources include non-domestic (industry, small power generators, transportation, etc.) and domestic (biofuel and fossil fuel combustion) sectors. LPSs are generally large power generators and iron or steel manufacturers. The domestic sectors contain monthly variations, but are distributed evenly throughout the day and week, while the non-domestic sectors and LPSs remain constant in time. In MICS-Asia II study, the area sources are allocated in the 1st layer, while LPSs are placed at the model layer close to 300 m (e.g., Han et al., 2008; Carmichael et al., 2008). In our study, LPSs are present in the 3rd layer for E_WD, E_D, and E_N which ignore the vertical allocations.

4. Temporal and vertical allocations of anthropogenic emissions

The TRACE-P anthropogenic emissions are separated into 4 categories: power generators (small power generators of non-domestic sectors and LPSs), industry (industry of non-domestic sectors), residential (domestic sectors), and transportation (transportation of non-domestic sectors). For each category and depending on chemical species, appropriate seasonal, day-of-week, and diurnal profiles are developed to first allocate emissions in time without changing the annual total. They are then redistributed in the vertical of several model layers conserving the column amount for the power generators, while assigned to the 1st layer for other categories.

4.1. Temporal allocations of emissions

The monthly variation profiles of the power and industry emissions for NO_x are adopted from Zhang et al. (2007). They were based on the monthly GDP data of China for the period of 1995-2004. The corresponding profiles for SO_2 and other species are from Olivier et al. (2003). Their use in China was shown to improve the urban air quality simulation over Nanjing (Wang et al.

ACCEPTED MANUSCRIPT

2007). The monthly profile of the residential emissions for each species is collected from Streets et al. (2003a) and Zhang et al. (2007). The profile for PM_{10} and $PM_{2.5}$ is the same as that for BC. The monthly profile of the transportation emissions is taken from Olivier et al. (2003). The same profile is assumed for all species.

The day-of-week variation profiles are constructed from the European Monitoring and Evaluation Programme (EMEP) emission inventory (http://aqm.jrc.it/eurodelta/) plus the Western Regional Air Partnership (WRAP, 2006) mobile source emission inventory. In EMEP, emissions are higher on weekdays than weekends by 25% for power generators and 35% for industry and residential sectors. Following Streets et al. (2003a) data, the transportation emissions are divided into light duty vehicles (LDVs: cars, light duty gasoline trucks, light duty diesel trucks, and motorcycles) and heavy duty vehicles (HDVs: buses, heavy duty gasoline trucks, heavy duty diesel trucks, and tractors). For major species, the emission factors of both LDVs and HDVs in Japan are similar to western countries (Kannari et al., 2007). The emission factors of LDVs and HDVs in China are also comparable because the dominant vehicle manufacturing technologies in China root in western technologies and automobiles emissions standards implemented in China have been equivalent to those executed in Europe since 2000 (Hao and Xie, 2007). Since EMEP lacks HDVs, WRAP divides LDVs into more subcategories too detailed for this study, the profile is adopted from EMEP for LDVs and from WRAP for HDVs. Both LDVs and HDVs profiles vary from Monday to Sunday. Differences between LDV and HDV emissions are large on weekends, but insignificant on weekdays. LDV emissions peak on Friday, with differences between weekdays and weekends similar to those of industry and residential sectors. HDVs are operated mainly during weekdays, with a steep decline of emissions on Friday and a much lower level on weekends.

ACCEPTED MANUSCRIPT

The diurnal variation profiles are based on Olivier et al. (2003) and the WRAP (2006) inventory. As shown in Fig. 2a, the power and industry emissions peak around noon, while the residential emissions are highest during the breakfast and dinner time and lowest at night. On weekdays, the LDV emissions exhibit two distinct peaks, corresponding to the morning and evening rush hours. In contrast, the HDV emissions closely match the working hours, increasing in the morning, staying high during mid-day, and decreasing after evening. On weekends, both LDV and HDV emissions peak around noon and remain high for several hours. The differentiation between LDVs and HDVs on weekdays is important, since their emission factors for each species differ largely. Figure 2b compares diurnal variations of weekday transportation emissions for 7 major pollutants. The percentages of LDVs and HDVs for each pollutant are derived from the U.S. EPA National Emissions Inventory 99 (NEI99). The transportation emissions of CO, NMVOC, and NH_3 are dominated by LDVs (~90%) and thus produce two significant peaks during the rush hours. On the other hand, HDVs contribute more than 50% of transportation emissions of $PM_{2.5}$ and PM_{10}, which vary little during daytime. The transportation emissions of NO_x and SO_2 also peak around the rush hours but with a smaller magnitude as both LDVs and HDVs are large contributors.

The day-of-week and diurnal variation profiles of each species for automobile emissions adopted here are similar to those used in previous model studies representing the emission inventories in China (Wang, et al., 2007) and Japan (Kannari et al., 2007).

When all source categories (power, industry, residential and mobile) combined, the differences of the 1st layer emissions averaged in daytime (nighttime) resulted from the day-of-week variation are small, within ±1.5% for each species. However, the differences caused by the diurnal variation are large. That alone allocates in the 1st layer SO_2 and NO_x emissions by 24%

and 26% higher (lower) in daytime (nighttime), respectively. The corresponding emissions for other species are 13-24% higher (lower) in daytime (nighttime).

4.2. Vertical allocations of emissions

Vertical distributions of emissions contain large uncertainties in most available inventories. In particular, the stack heights and associated plume-rise for point sources are not available outside North America. As such, the EMEP inventory distributes European emissions in the vertical based on very few bottom-up model studies (de Meij et al., 2006). This study derives the vertical profiles for East Asia based on the U.S. EPA NEI99 to allocate emissions of the power generators, including LPSs and small power generators, in different model layers. These profiles are derived from the stack heights and plume-rise calculations over the U.S., which were found comparable to those estimated in China and Japan (Woo et al. 2003). Although the applicability to East Asia has some inherent uncertainty, they represent an improvement over the common practice of putting power plant emissions in a single model layer. As shown in Table 3, the power generator emissions peak in the 3rd model layer for SO_2 and in the 2nd layer for others. Emissions are small near the surface and above 500 m for all pollutants.

Note that small power generators emissions are assigned totally to the 1st layer, and LPSs to the 3rd layer, in the set of the simulations excluding the vertical allocation (E_WD, E_D, and E_N). In contrast, they both are redistributed into several model layers in the set of the simulations including the vertical allocation (E_WDV, E_DV, and E_V). Thus, when summed over time in a month, the actual emissions in the 1st layer are identical among the simulations of each set but differ between the two sets. The vertical redistribution alone gives the 1st layer lower emissions of SO_2, NO_x, CO, NMVOC, NH_3, and PM_{10}, respectively, by 56, 19, 4, 8, 1, and 6%.

5. Effects of temporal and vertical allocations of emissions

ACCEPTED MANUSCRIPT

This section compares the six simulations described in section 2 for July 2001 to depict the individual and combined effects of temporal and vertical allocations of emissions on air quality modeling over East Asia. Since the total column emissions in July are identical, the simulations differ only in temporal and/or vertical redistributions of anthropogenic emissions. As compared with the control experiment E_N using the default monthly emissions, the complete simulation E_WDV including the day-of-week, diurnal and vertical allocations incorporates into the 1st layer daytime (8am-8pm) average emissions lower by 41% for SO_2, but higher by 11, 24, 14, 18, and 11% for NO_x, CO, NMVOC, NH_3, and PM_{10}. On the other hand, the nighttime (8pm-8am) average emissions for SO_2, NO_x, CO, NMVOC, NH_3, and PM_{10} are all reduced, respectively by 70, 44, 30, 31, 20, and 22%. As discussed early, these changes are mainly attributed to the diurnal and vertical allocations.

5.1. Effects on NO_2 and SO_2

Tables 4-5 summarize the statistics for daily mean surface NO_2 and SO_2 concentrations comparing against observations the six simulations using different emissions allocations. They are calculated separately for 4 sites in China and 10 sites in Japan due to different characteristics of pollutants and emissions. There is a total of 124 samples for NO_2 and SO_2 in China, and 223 (NO_2) and 291 (SO_2) samples in Japan. For both pollutants, Japan is much cleaner than China, with observed July mean NO_2, SO_2 concentrations of 1.61, 0.90 ppbv versus 6.56, 5.70 ppbv.

For NO_2 over both China and Japan, E_WDV is overall superior to other simulations, having the highest correlation and smallest mean (normalized) bias or gross (normalized) error. In opposite, E_N is the worst by all the measures. As compared with E_WDV, differences are minor for E_DV, depicting small effect by the emissions' day-of-week variation. In contrast, E_V produces a larger mean (normalized) bias and gross (normalized) error, suggesting a

ACCEPTED MANUSCRIPT

significant role of the emissions' diurnal variation. The largest increases in bias and error occur in E_WD, E_D and E_N, indicating the dominant impact of the emissions' vertical variation.

The WRF-Chem simulates SO_2 daily variations more realistically than NO_2 as all temporal correlations with observations are systematically higher. Nonetheless, the above conclusions for NO_2 are generally the same for SO_2. In particular, over both China and Japan, incorporation of the emissions' diurnal and vertical variations (E_WDV, E_DV) produces the most realistic SO_2 concentrations, while using the default emissions (E_N) is the worst by almost all the measures. Again, the emissions' the day-of-week variation has negligible effect. On the other hand, the vertical variation plays a pronounced role, causing systematically lower SO_2 concentrations over China by (2.15, 2.19, 1.89) ppbv in (E_WDV, E_DV, E_V) than (E_WD, E_D, E_N). As a result, the mean biases with and without the vertical allocation are opposite and comparable in magnitude. The differences in Japan are small due to the relatively low concentrations.

Note that the model result depends on the applicability of the USA vertical scaling profiles to East Asia. This is illustrated by another sensitivity experiment, where power generators of SO_2 emissions are allocated with 30, 30, 30, 5, and 5% into the low 5 model layers while keeping others the same as E_WDV. This new scaling yields more realistic surface SO_2 concentrations in China than E_WDV, with a larger temporal correlation (0.63) and smaller mean bias (0.2 ppbv) and gross error (0.9 ppbv). The improvement is relatively small in Japan, with the corresponding statistics of 0.95, 0.0 ppbv, and 0.3 ppbv. Thus, the E_WDV underestimation of surface SO_2 concentrations in China may result from uncertainty in the vertical allocation of emissions. The uncertainty reduction requires improved specifications of the stack parameters, including its height, diameter, and escape temperature.

ACCEPTED MANUSCRIPT

Table 6 summarizes the statistics for monthly mean surface NO_2 and SO_2 concentrations comparing gross spatial characteristics with observations. There are 16 sites in China, Japan, and Thailand for NO_2, and 24 sites in China, Japan, Russia, Thailand, and Vietnam for SO_2. For both NO_2 and SO_2, E_WDV produces the most realistic spatial variation across all EANET sites, while E_N is the worst. The emissions' vertical variation contributes the most to the improvement. Its neglect causes large overestimations of surface concentrations, with the net increases from (E_WDV, E_DV, and E_V) to (E_WD, E_D, E_N) by 0.66-0.95 ppbv (24-30%) for NO_2 and 1.39-1.56 ppbv (51-55%) for SO_2. The emissions' diurnal variation also plays an important role, while the effect from the day-of-week variation is minor. These results on the spatial pattern are consistent with the findings from the temporal characteristics (Tables 4-5).

Figure 3 compares with observations the NO_2 and SO_2 frequency distributions simulated by E_WDV, E_WD and E_N. They are based on daily mean concentrations at 4 sites in China and 10 sites in Japan. Over China, for low concentrations (<3 ppbv), the NO_2 frequency in all six simulations is much less than observations. This is identified with the model failure in capturing the low concentrations at rural site 2 (Jinyunshan) that locates nearby urban areas. The coarse grid spacing of the emissions inventory (0.5º) and the model (30-km) is insufficient to resolve the large gradients from high urban emissions/concentrations to low rural values (Carmichael et al., 2008; Han et al., 2008). For high concentrations (>12 ppbv), E_WDV is fairly realistic, while E_WD and E_N overestimate the frequency. For medium low concentrations (3-9 ppbv), E_WDV is also quite realistic, but large underestimations occur in other simulations. For medium high concentrations (9-12 ppbv), overestimations exist in all simulations, largest in E_WDV. The shape of the SO_2 frequency distribution is best simulated by E_WDV, while E_WD and E_N have systematic shifts toward higher concentrations. Over Japan, for both NO_2

ACCEPTED MANUSCRIPT

and SO_2, E_WDV is the most realistic, while others generate larger underestimations in the low range (<2 ppbv for NO_2, <0.5 ppbv for SO_2) and overestimations in the medium range (4-8 ppbv for NO_2, 1-2 ppbv for SO_2).

Figure 4 compares the NO_x and SO_2 diurnal cycles simulated by E_WDV, E_WD and E_N with observations available only at 10 sites in Japan. NO_x is the sum of NO and NO_2. As a key precursor, NO_x has a strong diurnal cycle that plays a significant role in O_3 formation, especially in the evening and early morning (Ying et al., 2009). Clearly, E_WDV simulates a much more realistic NO_x diurnal cycle than E_N, which has larger underestimations during afternoon-early evening but substantial overestimations from midnight to morning. The diurnal variation causes surface NO_x to increase largely during afternoon-early evening and decrease substantially from midnight to morning. On the other hand, the vertical variation reduces surface concentrations throughout the day. The simulated SO_2 diurnal cycle is also more realistic by E_WDV than E_N. In fact, the E_N result is almost opposite in phase to observations.

Figure 5a illustrates the geographic distribution of July mean NO_2 concentration differences of E_N from E_WDV. The differences are all positive since E_N allocates more NO_2 emissions in the 1st model layer than E_WDV. The differences are especially large in the major cities and industrial regions over China and Japan. They are about 3-7 ppbv over parts of northern China and major cities (e.g., Shenyang, Taiyuan, and Shanghai). The largest differences (~8 ppbv) are simulated in the Beijing metropolitan areas. The differences are up to 7 ppbv in Tokyo and Osaka in Japan.

Figure 5b shows the geographic distribution of July mean SO_2 concentration differences of E_N from E_WDV. Again, the differences are all positive since E_N allocates more SO_2 emissions in the 1st model layer than E_WDV. They are about 6~8 ppbv over northern and

ACCEPTED MANUSCRIPT

eastern China and Sichuan Basin, and up to 12~14 ppbv in Taiyuan and Chongqing. The largest differences over China reach 26 ppbv in Beijing and even greater in Shanghai. The differences over Japan are generally below 10 ppbv.

5.2. Effects on O_3

Table 7 summarizes the statistics for daily and monthly mean O_3 concentrations comparing respectively the temporal and spatial characteristics of the six simulations with observations. Measurements are currently available only from 10 sites in Japan, containing a total of 274 and 10 samples. All the statistics measures show that differences among the six simulations are small.

The frequency distribution of daily mean O_3 concentrations is also similar among the six simulations (not shown). They all overestimate the frequency in the intermediate range (40-60 ppbv) while agree well with observations for high concentrations (>80 ppbv). In addition, the total number of events when hourly surface O_3 concentrations exceed 80 ppbv is 61-66 for the six simulations, as compared with 73 for observations. WRF-Chem tends to underestimate the frequency of high O_3 episodes.

Figure 6 compares the diurnal cycles of surface O_3 concentrations simulated by E_WDV and E_N with observations at 10 sites in Japan. The other simulations are not shown as the differences are relatively small. The observed O_3 maximizes around 4 pm and minimizes around 8 am. Both E_WDV and E_N well simulate this phase change. They predict similar daytime O_3 concentrations, both overestimating observations by 4 ppbv. Larger differences (4-11%) between the two simulations exist for nighttime and early morning, with 2-3 ppbv higher by E_WDV. As suggested by Ying et al. (2009), the diurnal variation of NO_x emissions plays a significant role in the evening and early morning O_3 formation.

ACCEPTED MANUSCRIPT

Figure 7 compares the time evolutions of daily max 1-hr O_3 concentrations simulated by E_WDV and E_N with the NEMCC observations in Beijing. For consistency, they are given in the units (μg m^{-3}) of the observational data (Wang et al., 2009). The factor converting from units of μg m^{-3} to ppbv is approximately 2:1 for this case, albeit depending on instant surface air density. The daily E_N minus E_WDV differences exceed negative 10 μg m^{-3} (5 ppbv) in about half of July. On average over the month, the E_N and E_WDV biases from the observed (137.8) data are -6.8 and +2.2 μg m^{-3}, or about -3.4 and +1.1 ppbv, respectively. They are relatively small, especially for E_WDV. In addition, the model well reproduces the daily variations, having a temporal correlation with observations of 0.71 (E_N) and 0.76 (E_WDV). Both statistics indicate that E_WDV is slightly better than E_N.

Figure 8 depicts the geographic distributions of July mean E_N minus E_WDV differences in nighttime, daytime, daily, and max 1-hr surface O_3 concentrations. They are mostly negative, indicating that the model generates less O_3 by using E_N than E_WDV emissions. The nighttime decreases are large, with 4-8 ppbv over broad areas of northern, eastern, and central China where daily maximum 8-hr O_3 is also high (up to 80 ppbv, not shown). The largest reductions (-10 ppbv) occur in big cities, such as Beijing and Shenyang in China, and Tokyo and Osaka in Japan. The daytime decreases are smaller, with 2-4 ppbv in northern, eastern, and central China. As a result, the daily average differences follow the nighttime spatial pattern with smaller magnitudes. The differences in max 1-hr O_3 closely follow those in daytime average with slightly smaller magnitudes in northern China but higher in eastern and central China. The effects of emissions temporal allocations on O_3 shown here are similar to those depicted in Tao et al. (2004).

The above result indicates that the magnitude of the E_N minus E_WDV differences is larger at nighttime than daytime. This can be explained as follows. As compared with E_WDV, at night

ACCEPTED MANUSCRIPT

E_N allocates much larger NO_x emissions and thus produces higher surface NO_x concentrations (Fig. 4a). Due to the lack of photochemical O_3 formation at night, the greater NO_x concentrations titrate more O_3 in E_N. On the other hand, during daylight hours, the NO_x emissions differences are small. As a result, the NO_x concentrations are similar between E_N and E_WDV at daytime (Fig. 4a), and consequently, small changes in daytime surface O_3 concentrations are generated.

As compared with E_WDV, the differences for E_DV are very small, depicting that the emissions' day-of-week profiles have insignificant effect on O_3 production. On the other hand, the differences for E_V resemble closely those for E_N, indicating that the diurnal profiles have important impacts on daytime/nighttime and peak O_3 concentrations and contribute most to the results shown in Fig. 8. For E_WD, the largest negative differences are about 4 (3) ppbv at nighttime (daytime) in eastern and central China; they are generally smaller than those shown in Fig. 8, suggesting that the vertical profiles play a relatively weaker role.

6. Summary

We have developed fine temporal (seasonal, day-of-week, diurnal) and vertical allocations of anthropogenic emissions for the TRACE-P inventory depending on source categories (power, industry, residential, transportation) and chemical species. Their individual and combined impacts on East Asian air quality are evaluated by comparing six simulations for July 2001 using WRF-Chem with 30-km horizontal grid spacing against available surface measurements from EANET and NEMCC. When summed over the month and vertical column, total emissions for each species are identical for all simulations in each grid cell. Thus, the result differences among the simulations are attributed only to the temporal and vertical redistributions of emissions.

The surface pollutant concentrations depend critically on the emissions allocated in the 1st model layer. In that layer, the combination of the day-of-week, diurnal, and vertical allocations

ACCEPTED MANUSCRIPT

incorporates daytime (8am-8pm) average emissions lower by 41% for SO_2 but higher by 11% for NO_x. On the other hand, the nighttime (8pm-8am) average emissions are both reduced, by 70% for SO_2 and 44% for NO_x. The vertical redistribution alone decreases SO_2 and NO_x emissions by 56% and 19%, respectively. Because of the diurnal allocation, the emissions in the 1st layer during daytime (nighttime) are 24% and 26% higher (lower) for SO_2 and NO_x, respectively. In contrast, the differences due to the day-of-week variation are small, all within ±1.5% when averaged in daytime or nighttime. Corresponding changes are made to other species, including CO, NH_3, NMVOC, BC, OC, $PM_{2.5}$, and PM_{10}.

For the primary pollutants NO_2 and SO_2, the diurnal and vertical redistributions of emissions play essential roles, while the day-of-week variation is less important. When all the three allocations of emissions are incorporated, WRF-Chem best simulates the observed temporal and spatial characteristics of surface NO_2 and SO_2 concentrations. On the other hand, the simulation using the default monthly emissions with none of the refinements are the worst. The sensitivity is especially large in the major cities and industrial regions over broad areas of northern and eastern China and Japan, where the differences are 3-7 ppbv for NO_2 and 6-12 ppbv for SO_2.

For the secondary pollutant O_3, the temporal and spatial characteristics of surface concentrations in Japan are realistically simulated, with small differences in response to the emissions redistributions. The evolution of daily max 1-hr O_3 concentrations observed in Beijing is also well reproduced, with a slight improvement by including the new emissions allocations. On the other hand, the incorporation of all the day-of-week, diurnal, and vertical redistributions of emissions causes WRF-Chem to simulate surface O_3 concentrations higher by 4-8 ppbv at night and 2-4 ppbv in daytime (on average of the month) over broad areas of northern, eastern and central China. To this sensitivity, the diurnal redistribution contributes more than the other

ACCEPTED MANUSCRIPT

two. The result agrees with Ying et al. (2009) in that O_3 concentrations are sensitive to the diurnal variation of NO_x emissions, especially at night.

Our results suggest the essential need to develop more realistic diurnal and vertical allocations of anthropogenic emissions over East Asia. Their existing uncertainties and here demonstrated impacts on air quality modeling are particularly large in and around big cities and industrial areas. Only by using accurate emissions will credible model simulations be made for policy makers to determine cause-effect relationships and target sources for controlling air pollution problems.

Acknowledgments

We thank David G. Streets and Qiang Zhang at Argonne National Laboratory for providing the TRACE-P inventory data and Yang Zhang at North Carolina State University for the NEMCC measurements. We also thank two anonymous reviewers for constructive comments on the manuscript. We acknowledge the Acid Deposition Monitoring Network in East Asia (EANET) for the observational data, and the National Oceanic and Atmospheric Administration Forecast Systems Laboratory and the National Center for Supercomputing Applications at the University of Illinois at Urbana-Champaign for the supercomputing support. The research was partially supported by the United States Environmental Protection Agency Science to Achieve Results (STAR) award EPA RD-83337301-0 and the China Scholarship Council. The views expressed are those of the authors and do not necessarily reflect those of the sponsoring agencies or the Illinois State Water Survey.

ACCEPTED MANUSCRIPT

References

Akimoto, H., 2003. Global air quality and pollution. Science, 302, 1716-1719.

Carmichael, G.R., Sakurai, T., Streets, D., Hozumi, Y., Ueda, H., Park, S.U., Fung, C., Han, Z., Kajino, M., Engardt, M., Bennet, C., Hayami, H., Sartelet, K., Holloway, T., Wang, Z., Kannari, A., Fu, J., Matsuda, K., Thongboonchoo, N., Amann, M., 2008. MICS-Asia II: The model intercomparison study for Asia Phase II methodology and overview of findings. Atmospheric Environment, 42, 3468–3490.

de Meij, A., Krol, M., Dentener, F., Vignati, E., Cuvelier, C., Thunis, P., 2006. The sensitivity of aerosol in Europe to two different emission inventories and temporal distribution of emissions. Atmospheric Chemistry and Physics, 6, 4287-4309.

EANET, 2001. Data Report on the Acid Deposition in the East Asian Region 2001. (available at http://www.eanet.cc/product/datarep/datarep01/datarep01_dry.pdf)

Fast, J.D., Gustafson Jr., W.I., Easter, R.C., Zaveri, R.A., Barnard, J.C., Chapman, E.G., Grell, G.A., Peckham, S.E., 2006. Evolution of ozone, particulates, and aerosol direct radiative forcing in the vicinity of Houston using a fully coupled meteorology-chemistry-aerosol model. Journal of Geophysical Research, 111(D21305), doi:10.1029/2005JD006721.

Grell, G.A., Peckham, S.E., Schmitz, R., McKeen, S.A., Frost, G., Skamarock, W.C., Eder, B., 2005. Fully coupled "online" chemistry within the WRF model. Atmospheric Environment, 39, 6957–6975.

Guenther, A., Zimmerman, P., Wildermuth, M., 1994. Natural volatile organic compound emission rate estimates for U.S. woodland landscapes. Atmospheric Environment, 28, 1197-1210.

ACCEPTED MANUSCRIPT

Han, Z., Sakurai, T., Ueda, H., Carmichael, G.R., Streets, D., Hayami, H., Wang, Z., Holloway, T., Engardt, M., Hozumi, Y., Park, S.U., Kajino, M., Sartelet, K., Fung, C., Bennet, C., Thongboonchoo, N., Tang, Y., Chang, A., Matsuda, K., Amann, M., 2008. MICS-Asia II: Model intercomparison and evaluation of ozone and relevant species. Atmospheric Environment, 42, 3491-3509.

Hao, C., Xie, S., 2007. Estimation of vehicular emission inventories in China from 1980 to 2005. Atmospheric Environment, 41, 8963-8979.

Jacob, D.J., Logan, J.A., Murti, P.P., 1999. Effect of rising Asian emissions on surface ozone in the United States. Geophysical Research Letters, 26, 2175-2178.

Kajino, M., Ueda, H., Satsumabayashi, H., An, J., 2004. Impacts of the eruption of Miyakejima Volcano on air quality over far east Asia. Journal of Geophysical Research, 109(D21204), doi:10.1029/2004JD004762.

Kannari, A., Tonooka, Y., Baba, T., Murano, K., 2007. Development of multiple-species 1 km × 1 km resolution hourly basis emissions inventory for Japan. Atmospheric Environment, 41, 3428-3439.

Kurata, G., Carmichael, G.R., Streets, D.G., Kitada, T., Tang, Y., Woo, J.-H., Thongboonchoo, N., 2004. Relationships between emission sources and air mass characteristics in East Asia during the TRACE-P period. Atmospheric Environment, 38, 6977–6987.

Ohara, T., Akimoto, H., Kurokawa, J., Horii, N., Yamaji, K., Yan, X., Hayasaka, T., 2007. An Asian emission inventory of anthropogenic emission sources for the period 1980-2020. Atmospheric Chemistry and Physics, 7, 4419-4444.

ACCEPTED MANUSCRIPT

Olivier, J., Peters, J., Granier, C., Pétron, G., Müller, J.F., Wallens, S., 2003. Present and future surface emissions of atmospheric compounds. POET Report #2, EU project EVK2-1999-00011.

Placet, M., Mann, C.O., Gilbert, R.O., Niefer, M.J., 2000. Emissions of ozone precursors from stationary sources: a critical review. Atmospheric Environment, 34, 2183-2204.

Stockwell, W.R., Kirchner, F., Kuhn, M., Seefeld, S., 1997. A new mechanism for regional atmospheric chemistry modeling. Journal of Geophysical Research, 102(D22), 25847–25879.

Streets, D.G., Bond, T.C., Carmichael, G.R., Fernandes, S.D., Fu, Q., He, D., Klimont, Z., Nelson, S.M., Tsai, N.Y., Wang, M.Q., Woo, J.-H., Yarber, K.F., 2003a. An inventory of gaseous and primary aerosol emissions in Asia in the year 2000. Journal of Geophysical Research, 108(D21), 8809, doi:10.1029/2002JD003093.

Streets, D.G., Yarber, K.F., Woo, J.-H., Carmichael, G.R., 2003b. Biomass burning in Asia: Annual and seasonal estimates and atmospheric emissions. Global Biogeochemical Cycles, 17(4), 1099, doi:10.1029/2003GB002040.

Tao, Z., Larson, S.M., Williams, A., Caughey, M., Wuebbles, D.J., 2004. Sensitivity of regional ozone concentrations to temporal distribution of emissions. Atmospheric Environment, 38, 6279-6285.

Wang, K., Zhang, Y., Jang, C., Phillips, S., Wang, B., 2009. Modeling intercontinental air pollution transport over the trans-Pacific region in 2001 using the Community Multiscale Air Quality modeling system. Journal of Geophysical Research, 114(D04307), doi:10.1029/2008JD010807.

ACCEPTED MANUSCRIPT

Wang, X., Mauzerall, D.L., Hu, Y., Russell, A.G., Larson, E.D., Woo, J.-H., Streets, D.G., Guenther, A., 2005. A high-resolution emission inventory for eastern China in 2000 and three scenarios for 2020. Atmospheric Environment, 39, 5917–5933.

Wang, X., Jiang, W., Liu, H., Wang, Y., Zhang, Y., 2007. Numerical simulation study on the effect of major industrial sources in Nanjing on urban air quality. Research of Environmental Sciences, 20(3), 33-43, (in Chinese).

Wesely, M.L., 1989. Parameterization of surface resistance to gaseous dry deposition in regional-scale numerical models. Atmospheric Environment, 23, 1293–1304.

Woo, J.-H., Baek, J.M., Kim, J.-W., Carmichael, G.R., Thongboonchoo, N., Kim, S.T., An, J.H., 2003. Development of a multi-resolution emission inventory and its impact on sulfure distribution for Northeast Asia. Water, Air and Soil Pollution, 148, 259-278.

WRAP, 2006. WRAP Mobile Source Emission Inventories Update Final Report. (Available at http://www.wrapair.org/forums/ef/UMSI/0606_WRAP_Mobile_Source_EI_Final_Report.pdf)

Ying, Z., Tie, X., Li, G. 2009. Sensitivity of ozone concentrations to diurnal variations of surface emissions in Mexico City: A WRF/Chem modeling study. Atmospheric Environment, 43, 851-859.

Zhang, Q., Streets, D.G., He, K., Wang, Y., Richter, A., Burrows, J.P., Uno, I., Jang, C,J., Chen, D., Yao, Z., Lei, Y., 2007. NO_x emission trends for China, 1995–2004: The view from the ground and the view from space. Journal of Geophysical Research, 112(D22306), doi:10.1029/2007JD008684.

ACCEPTED MANUSCRIPT

Figure Caption

Figure 1. WRF-Chem model computational domain and the locations of the EANET monitoring sites, labeled by their respective IDs (see Table 2).

Figure 2. The diurnal variations of emissions for four source categories (a) and transportation emissions for seven primary species (b).

Figure 3. The frequency distribution of daily mean surface NO_2 (left) and SO_2 (right) concentrations observed (OBS) and simulated by E_WDV, E_WD, and E_N at the EANET sites in China (top) and in Japan (bottom) for July of 2001.

Figure 4. The diurnal cycles of surface NO_x (a) and SO_2 (b) concentrations observed (OBS) and simulated by E_WDV, E_WD, and E_N at the EANET sites in Japan for July of 2001.

Figure 5. The July mean E_N minus E_WDV differences (ppbv) of surface NO_2 (a) and SO_2 (b) concentrations.

Figure 6. The diurnal cycle of surface O_3 concentrations observed (OBS) and simulated by E_WDV and E_N at the EANET sites in Japan for July of 2001.

Figure 7. The evolution of the daily max 1-hr O_3 concentrations in Beijing for July of 2001.

Figure 8. The July mean E_N minus E_WDV differences (ppbv) of surface O_3 concentrations for average of nighttime (a), daytime (b), daily (c), and daily max 1-hr (d).

ACCEPTED MANUSCRIPT

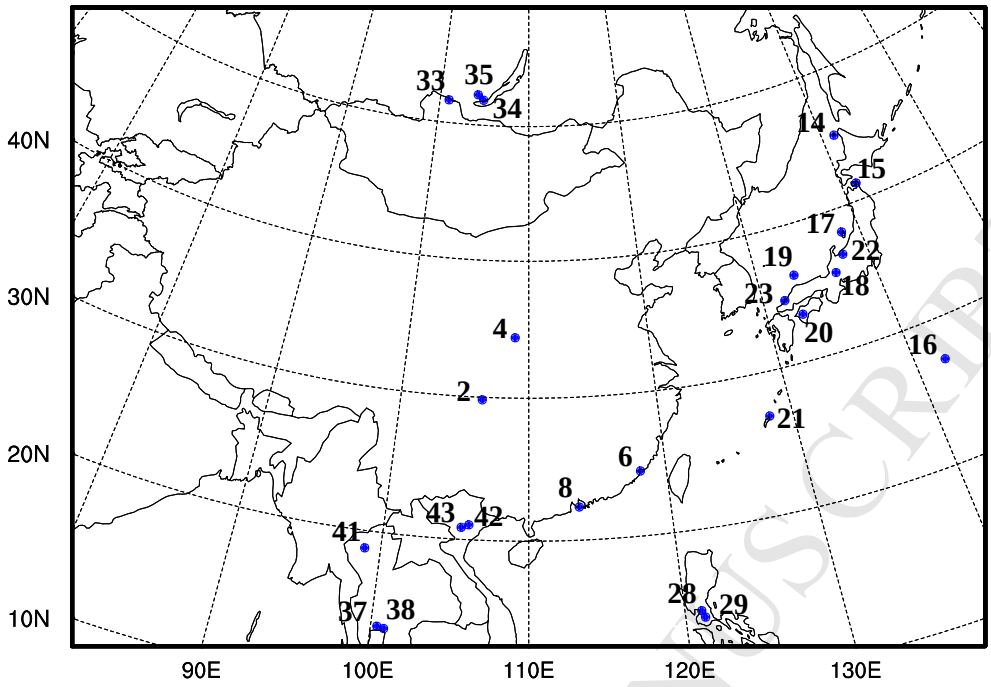

Figure 1. WRF-Chem model computational domain and the locations of the EANET monitoring sites, labeled by their respective IDs (see Table 2).

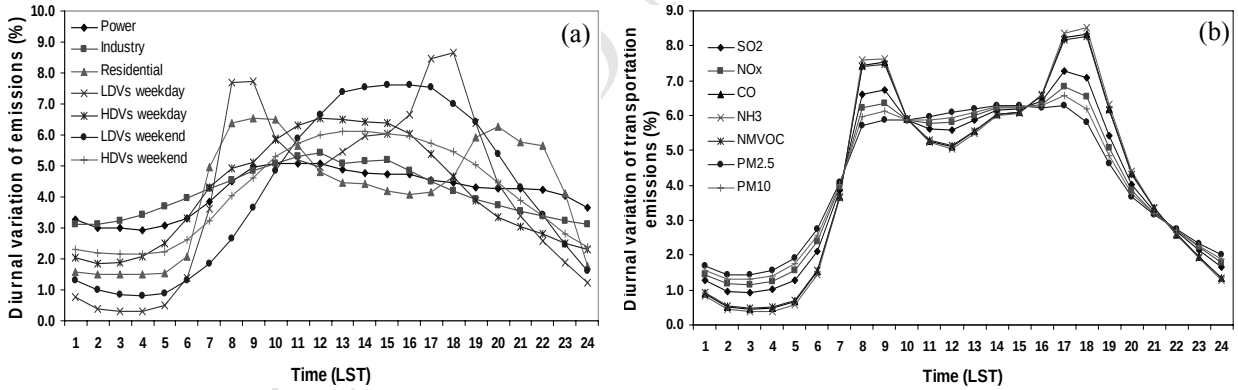

Figure 2. The diurnal variations of emissions for four source categories[a] (a) and transportation emissions for seven primary species (b).

[a]Source from Olivier et al. (2003) and the WRAP (2006).

ACCEPTED MANUSCRIPT

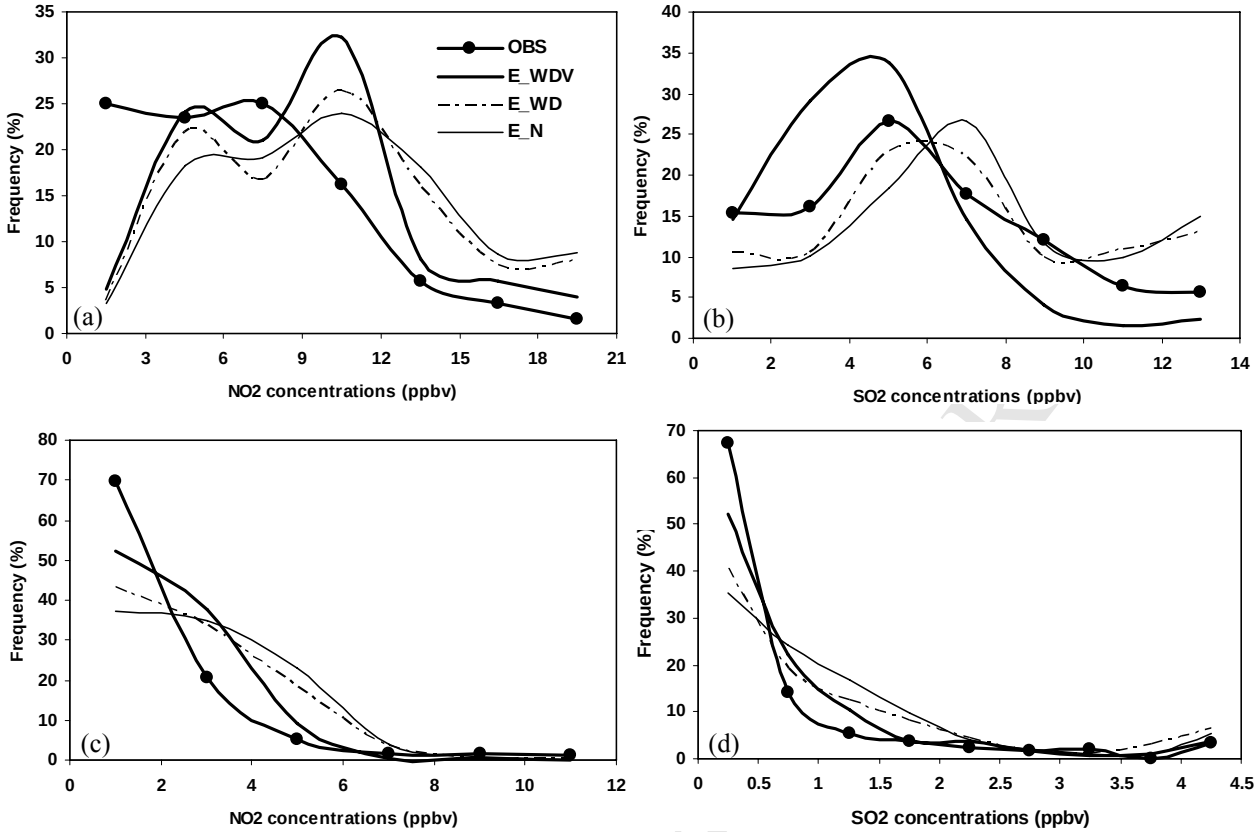

Figure 3. The frequency distribution of daily mean surface NO_2 (left) and SO_2 (right) concentrations observed (OBS) and simulated by E_WDV, E_WD, and E_N at the EANET sites in China (top) and in Japan (bottom) for July of 2001.

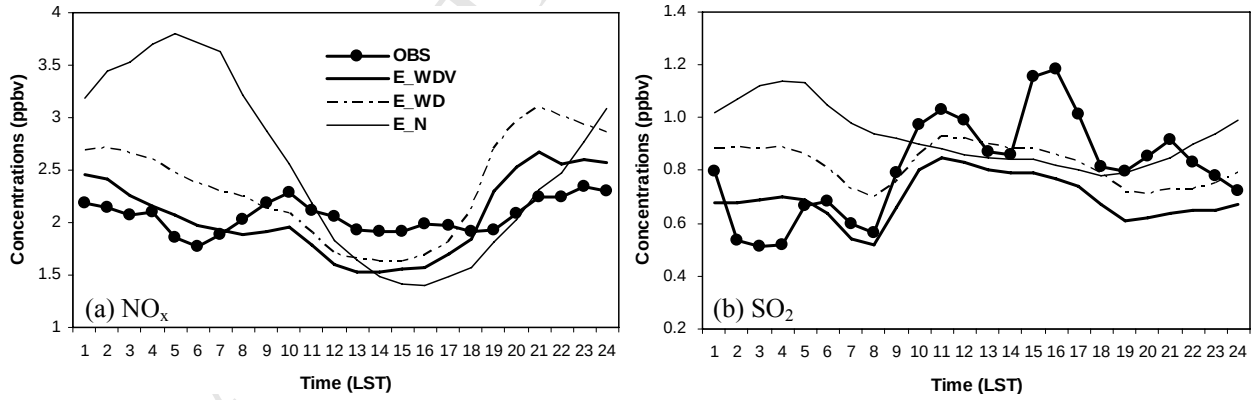

Figure 4. The diurnal cycles of surface NO_x (a) and SO_2 (b) concentrations observed (OBS) and simulated by E_WDV, E_WD, and E_N at the EANET sites in Japan for July of 2001.

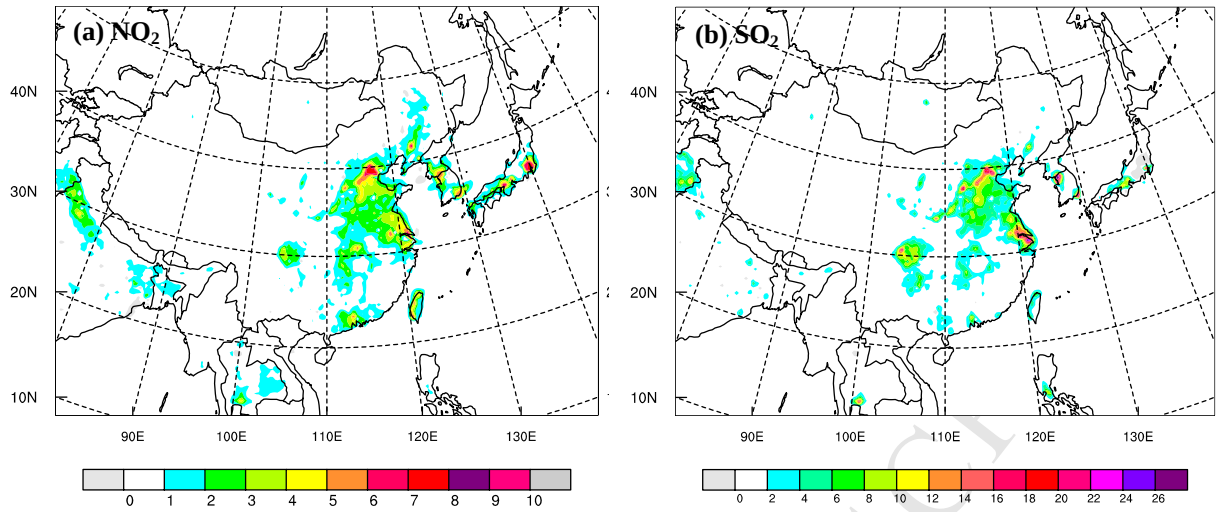

Figure 5. The July mean E_N minus E_WDV differences (ppbv) of surface NO_2 (a) and SO_2 (b) concentrations.

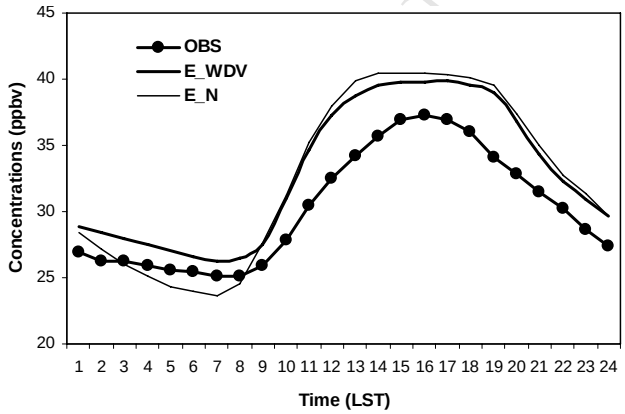

Figure 6. The diurnal cycle of surface O_3 concentrations observed (OBS) and simulated by E_WDV and E_N at the EANET sites in Japan for July of 2001.

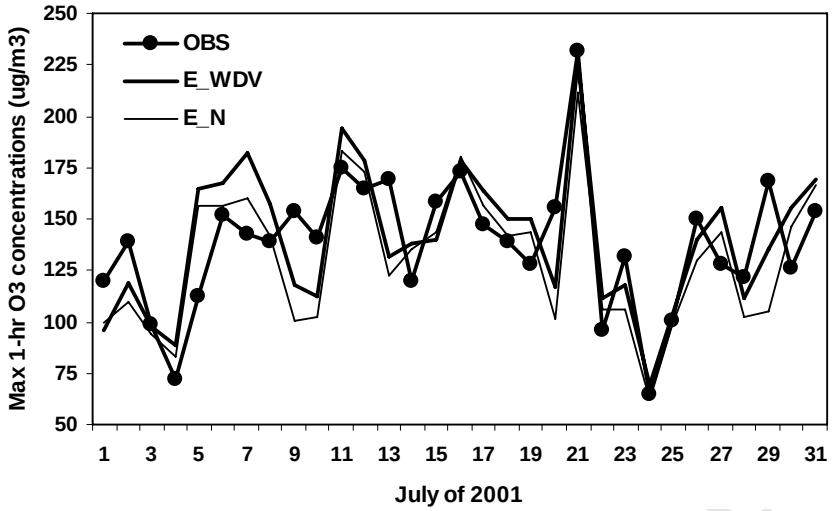

Figure 7. The evolution of the daily max 1-hr O_3 concentrations in Beijing for July of 2001.

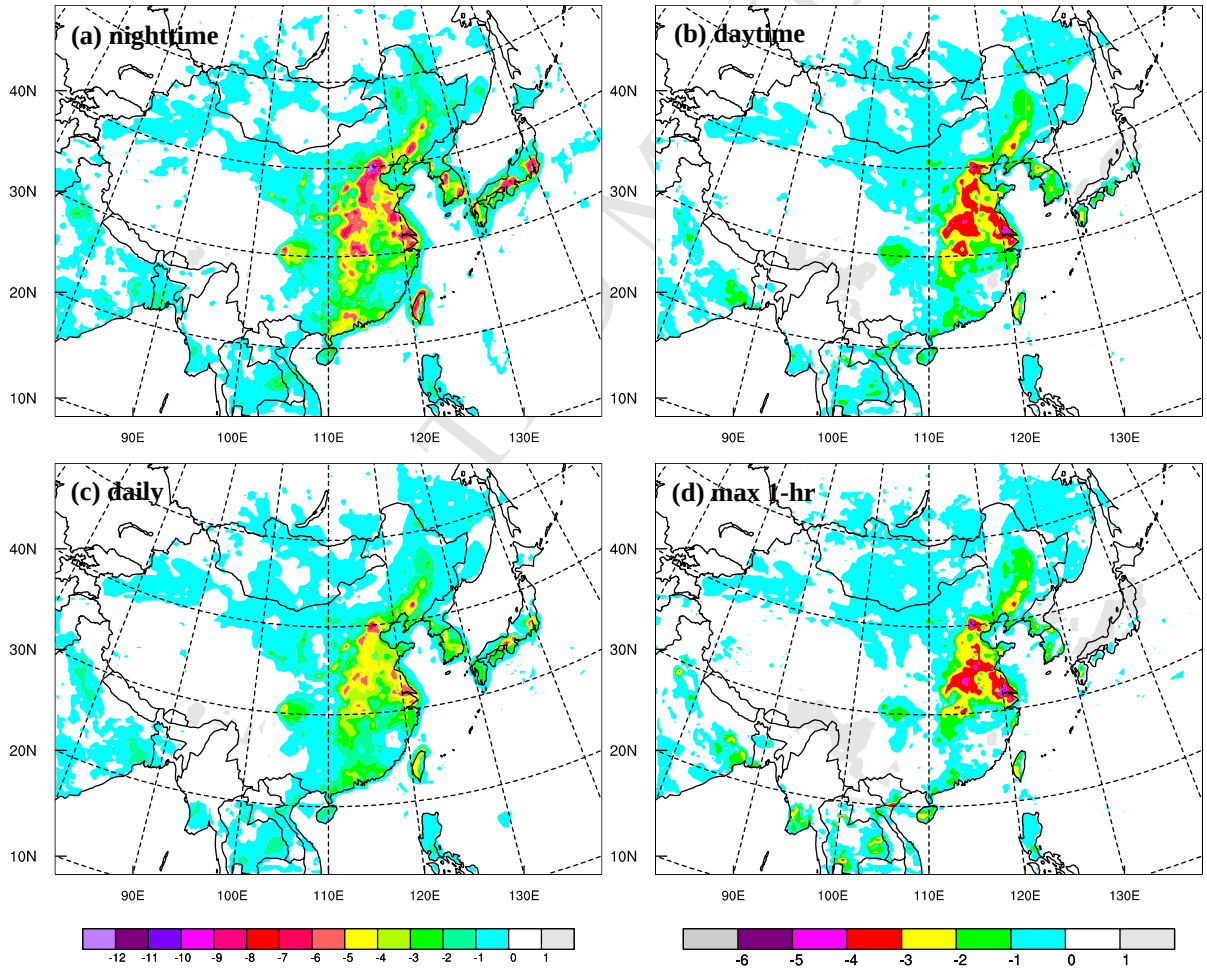

Figure 8. The July mean E_N minus E_WDV differences (ppbv) of surface O_3 concentrations for average of nighttime (a), daytime (b), daily (c), and daily max 1-hr (d).

Table 1. The description of the model simulations for the incorporation of anthropogenic emissions with (√) or without (×) the day-of-week (W), diurnal cycle (D) and vertical (V) variation profiles. Simulation N depicts the control experiment based on the monthly emissions with none of the day-of-week, diurnal and vertical allocations developed in this study.

Emissions profiles	Simulation identification					
	WDV	DV	V	WD	D	N
Day-of-week variation	√	×	×	√	×	×
Diurnal variation	√	√	×	√	√	×
Vertical variation	√	√	√	×	×	×

Table 2. Description of monitoring sites with available datasets

Database	Country	Site ID[a]	Site Name	Location	Characteristics	Available Data
EANET	China	2	Jinyunshan	29.8º N, 106.4º E	Rural	Daily average (NO_2, SO_2)
		4	Weishuiyuan	34.4º N, 108.9º E	Rural	
		6	Hongwen	24.5º N, 118.1º E	Urban	
		8	Xiang Zhou	22.3º N, 113.6º E	Urban	
	Japan	14	Rishiri	45.1º N, 141.2º E	Remote	Hourly (NO_2, NO, SO_2, O_3)
		15	Tappi	41.3º N, 141.4º E	Remote	
		16	Ogasawara	27.1º N, 142.2º E	Remote	
		17	Sado-seki	38.3º N, 138.4º E	Remote	
		18	Happo	36.7º N, 137.8º E	Remote	
		19	Oki	36.3º N, 133.2º E	Remote	
		20	Yusuhara	33.4º N, 132.9º E	Remote	
		21	Hedo	26.9º N, 128.3º E	Remote	
		22	Ijira	35.6º N, 136.7º E	Rural	
		23	Banryu	34.7º N, 131.8º E	Urban	
	Philippines	28	Metro Manila	14.6º N, 121.1º E	Urban	Monthly average (NO_2, SO_2)
		29	Los Banos	14.2º N, 121.3º E	Rural	
	Russia	33	Mondy	51.7º N, 101.0º E	Remote	
		34	Listvyanka	51.9º N, 104.9º E	Rural	
		35	Irkutsk	52.2º N, 104.3º E	Urban	
	Thailand	37	Bangkok	13.8º N, 100.5º E	Urban	
		38	Samutprakarn	13.7º N, 100.6º E	Urban	
		41	Mae Hia	18.8º N, 98.9º E	Rural	
	Vietnam	42	Hanoi	21.0º N, 105.9º E	Urban	
		43	Hoa Binh	20.8º N, 105.3º E	Rural	
NEMCC	China	Beijing[b]		39.9º N, 116.4º E	Urban	Max 1-hr O_3

[a]EANET site ID numbers follow Carmichael et al. (2008).
[b]NEMCC observed max 1-hr O_3 concentrations are averaged over 8 sites in Beijing, which were post-processed by Tsinghua University (Wang et al., 2009).

ACCEPTED MANUSCRIPT

Table 3. Vertical distribution of power generator emissions: percentage of each species allocated to the vertical layers of the WRF-Chem model (given as heights of layers)

	Height of Emission Layer (Unit: m)				
Species	0-76	76-153	153-308	308-547	547-871
SO_2	5	30	35	25	5
NO_x	5	40	25	25	5
CO	5	70	20	5	
NH_3	5	75	15	5	
NMVOC	5	85	10		
$PM_{2.5}$	5	45	25	20	5
PM_{10}	5	55	20	15	5
BC	5	65	20	10	
OC	5	70	15	10	

Table 4. The statistics of daily mean surface NO_2 concentrations for July of 2001 based on instant averages separately over 4 sites in China and 10 sites in Japan comparing the temporal characteristics of the six simulations with observations. Values in bold are the observed average concentrations (ppbv).

Site	Statistics	(Unit)	E_WDV	E_DV	E_V	E_WD	E_D	E_N
China	R		0.49	0.47	0.48	0.47	0.46	0.46
6.56	MB	(ppbv)	0.46	0.45	0.74	1.75	1.70	2.18
	NB	(%)	9.6	9.6	14.0	28.6	27.9	35.5
	GE	(ppbv)	1.54	1.62	1.92	2.21	2.18	2.40
	NE	(%)	23.8	24.9	30.5	35.7	34.8	41.1
Japan	R		0.38	0.38	0.38	0.37	0.38	0.38
1.61	MB	(ppbv)	-0.02	-0.02	0.12	0.30	0.33	0.48
	NB	(%)	14.7	14.9	24.0	38.7	39.6	51.0
	GE	(ppbv)	0.57	0.59	0.62	0.65	0.66	0.72
	NE	(%)	40.8	43.6	47.1	52.6	53.4	59.9

ACCEPTED MANUSCRIPT

Table 5. Same as Table 4 except for SO_2.

Site	Statistics	(Unit)	E_WDV	E_DV	E_V	E_WD	E_D	E_N
China	R		0.58	0.57	0.55	0.56	0.55	0.55
5.70	MB	(ppbv)	-1.09	-1.13	-0.38	1.06	1.06	1.51
	NB	(%)	-10.3	-10.9	3.8	27.9	28.1	39.6
	GE	(ppbv)	1.60	1.62	1.70	1.82	1.83	2.01
	NE	(%)	25.0	26.3	31.4	38.2	38.5	50.2
Japan	R		0.96	0.95	0.94	0.93	0.93	0.94
0.90	MB	(ppbv)	-0.10	-0.11	-0.05	-0.01	0.01	0.07
	NB	(%)	21.8	20.6	27.1	38.4	41.9	52.9
	GE	(ppbv)	0.29	0.28	0.30	0.32	0.33	0.36
	NE	(%)	39.5	38.8	42.1	50.6	54.3	66.0

Table 6. The statistics of monthly mean surface NO_2 and SO_2 concentrations for July of 2001 comparing the spatial characteristics of the six simulations with observations at the EANET sites with available data. Values in bold are the observed average concentrations (ppbv).

Species	Statistics	(Unit)	E_WDV	E_DV	E_V	E_WD	E_D	E_N
NO_2	R		0.92	0.91	0.91	0.92	0.91	0.90
4.67	MB	(ppbv)	0.19	0.16	0.30	0.85	0.88	1.25
	NB	(%)	9.8	9.5	12.6	33.8	36.1	42.9
	GE	(ppbv)	1.18	1.18	1.22	1.41	1.46	1.55
	NE	(%)	37.6	38.5	40.1	50.4	51.9	58.6
SO_2	R		0.95	0.95	0.91	0.85	0.84	0.81
2.17	MB	(ppbv)	-0.34	-0.35	-0.1	1.05	1.15	1.46
	NB	(%)	-11.8	-12.1	3.5	38.9	43.0	58.6
	GE	(ppbv)	0.49	0.51	0.62	1.46	1.51	1.81
	NE	(%)	37.1	39.6	44.6	63.6	65.5	79.8

ACCEPTED MANUSCRIPT

Table 7. The statistics of daily and monthly mean surface O_3 concentrations for July of 2001 comparing, respectively, the temporal (*upper*) and spatial (*lower*) characteristics of the six simulations with observations at 10 sites in Japan. Values in bold are the observed average concentrations (ppbv).

Japan	Statistics	(Unit)	E_WDV	E_DV	E_V	E_WD	E_D	E_N
Daily mean	R		0.67	0.64	0.65	0.65	0.65	0.66
30.10	MB	(ppbv)	2.87	2.59	2.26	2.79	2.69	2.32
	NB	(%)	6.3	6.2	6.0	6.3	6.2	6.1
	GE	(ppbv)	4.33	4.38	4.30	5.12	4.98	4.55
	NE	(%)	9.4	9.5	9.3	11.9	11.6	10.1
Monthly mean	R		0.85	0.84	0.84	0.82	0.81	0.82
30.10	MB	(ppbv)	2.88	2.60	2.26	2.79	2.68	2.36
	NB	(%)	6.8	6.5	5.8	6.8	6.6	6.3
	GE	(ppbv)	4.98	4.66	4.60	5.41	5.22	4.91
	NE	(%)	10.2	9.9	9.7	12.3	12.0	10.8

ACCEPTED MANUSCRIPT